

Density profiles of the exclusive queueing process

Chikashi Arita* and Andreas Schadschneider†

Abstract

The exclusive queueing process (EQP) incorporates the exclusion principle into classic queueing models. It can be interpreted as an exclusion process of variable system length. Here we extend previous studies of its phase diagram by identifying subphases which can be distinguished by the number of plateaus in the density profiles. Furthermore the influence of different update procedures (parallel, backward-ordered, continuous time) is determined.

1 Introduction

Queueing theory is one of the most important topics in the field of operations research [1, 2, 3]. It has a broad spectrum of applications ranging from telecommunications to traffic engineering and supply chains. One of the simplest queueing processes is the so-called M/M/1 model, where customers enter the system with probability α and leave the system with probability β at one server. The current state of the M/M/1 queueing process is completely specified by the number of customers. The system converges to a stationary state with a finite number of customers when $\alpha < \beta$ whereas the number of waiting customers diverges for $\alpha > \beta$.

A feature which seems to be important for pedestrian queues and other traffic applications is the excluded-volume effect: pedestrians can proceed only when there is enough space in front of them [4]. This is e.g. seen in queues at the check-in at airports where passengers have to move the luggage when moving forward. However, standard queueing models like the M/M/1 model neglect the excluded-volume effect, and do not have a spatial structure. Then the length L of the system is given by the number of waiting customers N (if customers have unit length) and the density is constant in space ($\rho = N/L = 1$).

The “exclusive queueing process” (EQP) was introduced in [5, 6] to investigate how the excluded volume affects queues. It is obtained by modifying the input procedure of the one-dimensional totally asymmetric simple exclusion process (TASEP) with the ordinary “open boundary condition.” Customers are injected always at the end of the queue, called left end in the following, i.e. behind the last customer waiting (Fig. 1). This is in contrast to the usual open TASEP where the input always happens at the same site, irrespective of the occupation of the other sites. The output is not changed compared to the usual open TASEP: in both models customers are extracted at the right end (the server) which is fixed.

The EQP is not the only variant of the TASEP on a dynamic lattice. An earlier example is the dynamically extending exclusion process (DEEP) introduced in

*Institut de Physique Théorique, CEA Saclay. chikashi.arita@cea.fr

†Institut für Theoretische Physik, Universität zu Köln. as@thp.uni-koeln.de

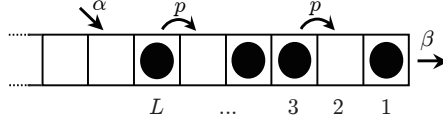


Figure 1: Exclusive queueing process.

[7, 8, 9, 10] as a model for fungal growth. In contrast to the EQP, the DEEP has no mechanism for reducing the system length and therefore the length of the system is always diverging. Other possible biological applications are length-regulation of microtubules [12] and bacterial flagellar growth [13].

The state space of the EQP is the set of configurations of the customers. It is more precisely given as

$$S = \{\tau = 1\tau_{L-1} \cdots \tau_1 | L \in \mathbb{Z}_{\geq 0}, \tau_j = 0, 1\}, \quad (1)$$

where $\tau = 0, 1$ for $L = 0, 1$, respectively. The state $\tau = 1\tau_{L-1} \cdots \tau_1 \in S \setminus \{\emptyset\}$ corresponds to the customer configuration where each site j is occupied or empty according to $\tau_j = 1$ or 0 , and L defines the length of the system. The symbol \emptyset corresponds to the state “no customer in the system.” We denote the number of customers ($\#(\tau_j = 1)$) by N for a given state $\tau = 1\tau_{L-1} \cdots \tau_1$. Each customer enters the system, hops and leaves the system as

$$\begin{aligned} \emptyset &\rightarrow 1 && \text{with probability } \alpha, \\ 1 \cdots &\rightarrow 11 \cdots && \text{with probability } \alpha, \\ \cdots 10 \cdots &\rightarrow \cdots 01 \cdots && \text{with probability } p, \\ \cdots 1 &\rightarrow \cdots 0 && \text{with probability } \beta. \end{aligned} \quad (2)$$

The local update rules (2) are not sufficient to specify the dynamics fully. In addition the sequence in which the rules are applied to the sites or particles needs to be defined. Here we consider two discrete-time updates (parallel and backward sequential updates) and a continuous-time dynamics where the parameters α, β and p are transition rates (not probabilities).

In [5, 14], exact stationary states for the continuous-time case and the parallel-update case were constructed as matrix product states based on the known forms for the corresponding TASEPs with a fixed length [15, 16]. The phase boundary between the convergent and divergent phases was found to be modified compared to the classical M/M/1 queue. In particular, for the convergence to the stationary states, the injection rate (or probability) α cannot be bigger than the maximal current of the TASEP, i.e. “the queue itself is a bottleneck” as well as the server.

In [17], the phase diagram was analyzed in more detail. The convergent and divergent phases are both further subdivided in two subphases analogous to the maximal current and high-density phases of the TASEP. Furthermore time dependent properties were investigated. However the asymptotic form of the velocity for the growth of L in the divergent phase was left as an open problem. In this article we will clarify this point, giving density profiles with help of Monte Carlo simulations. (In the case where the customer hopping is deterministic ($p = 1$), an exact “dynamical state” in matrix product form exists which enables us to rigorously derive the behavior of $\langle L_t \rangle$ and $\langle N_t \rangle$ [18].)

This article is organized as follows. In Section 2, we define the EQPs with various updates in more detail. The phase diagrams are derived and their relation with classical queueing processes is discussed. In Section 3, based on simulation results we characterize further subphases of the divergent phases according to the shapes of the density profiles. In Section 4, we investigate the EQPs on the critical line separating the divergent and convergent phases. Finally, we give a summary and conclusions of this article in Section 5.

2 Update rules

The TASEP is a prototypical model of stochastic interacting particle systems. It has been studied intensively in the last decades both from the view of nonequilibrium statistical physics [19, 20, 21, 4] and mathematics (see e.g. [22]). Similar to the TASEP with the ordinary open boundary condition [23] one can study the EQP with different update schemes. In the next two subsections we define two discrete-time EQPs and determine their phase diagrams. These are divided into four phases according to their asymptotic lengths (convergent vs. divergent) and the parameter-dependence of the outflows. Then we consider special cases and limits including the continuous-time EQP.

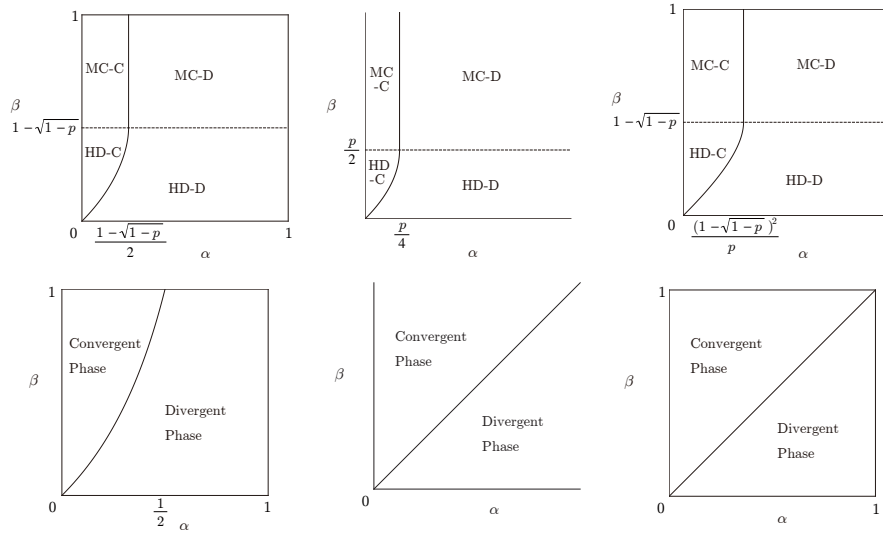


Figure 2: The phase diagrams of various queueing processes: the parallel EQP (top-left), the continuous-time EQP (top-middle), the backward EQP (top-right), the rule 184 CA with stochastic boundaries (bottom-left), the continuous-time M/M/1 (bottom-middle) and the discrete M/M/1 (bottom-right). The relations among the phase diagrams can be seen by (15). For example the bottom-left is obtained by setting $p = 1$ in the top-left.

2.1 Parallel update

In [6, 14, 17, 18], the EQP with the parallel update rule, which we call parallel EQP shortly, was investigated. In the parallel dynamics all sites are updated simultaneously,

e.g.

$$\begin{aligned}
101011 &\rightarrow 1011010 && \text{with probability } \alpha \times p \times (1-p) \times \beta, \\
111011 &\rightarrow 110111 && \text{with probability } (1-\alpha) \times p \times (1-\beta), \\
\emptyset &\rightarrow \emptyset && \text{with probability } 1-\alpha.
\end{aligned} \tag{3}$$

The current-density relation for the TASEP with the parallel update and the periodic boundary condition is given by [24, 25]

$$J_{\parallel}(\rho) = \frac{1 - \sqrt{1 - 4p\rho(1-\rho)}}{2}, \tag{4}$$

which is also true for the ordinary open boundary condition [16]. The “critical line” that separates the parameter space into divergent and convergent phases is given by $\alpha = J_{\parallel}(\rho_{\parallel})$, where

$$J_{\parallel}(\rho_{\parallel}) = \begin{cases} \frac{\beta(p-\beta)}{p-\beta^2} & (0 < \beta \leq \beta_c), \\ \frac{1-\sqrt{1-p}}{2} & (\beta_c < \beta \leq 1), \end{cases} \quad \text{where } \rho_{\parallel} = \begin{cases} \frac{p-\beta}{p-\beta^2} & (0 < \beta \leq \beta_c), \\ \frac{1}{2} & (\beta_c < \beta \leq 1), \end{cases} \tag{5}$$

with $\beta_c = 1 - \sqrt{1-p}$. When $\alpha < J_{\parallel}(\rho_{\parallel})$, the system converges to a stationary state which has a matrix product form [14]. The number of customers $\langle N_t \rangle$ decreases approximately linearly in time as

$$\langle N_t \rangle \sim (\alpha - J_{\parallel}(\rho_{\parallel}))t + \langle N_0 \rangle \tag{6}$$

while $t \lesssim \frac{\langle N_0 \rangle}{J_{\parallel}(\rho_{\parallel}) - \alpha}$ starting from a sufficiently large $\langle N_0 \rangle$ at time $t = 0$. The quantity $J_{\parallel}(\rho_{\parallel})$ is actually the customer current through the right end, i.e. the outflow. The system length exhibits a similar behavior

$$\langle L_t \rangle \sim \frac{\alpha - J_{\parallel}(\rho_{\parallel})}{\rho_{\parallel}}t + \langle L_0 \rangle, \tag{7}$$

where the density profile is almost flat with the bulk density ρ_{\parallel} . In view of the form (5), we call the region $\alpha < J_{\parallel}(\rho_{\parallel})$ with $\beta > \beta_c$ “maximal-current-convergent (MC-C) phase”, and $\alpha < J_{\parallel}(\rho_{\parallel})$ with $\beta < \beta_c$ “high-density-convergent (HD-C) phase”.

When $\alpha > J_{\parallel}(\rho_{\parallel})$, the system does not have a stationary state, and $\langle N_t \rangle$ and $\langle L_t \rangle$ diverge linearly in time. For $\langle N_t \rangle$, the form (6) is valid and we have the asymptotic behavior

$$\langle N_t \rangle \simeq (\alpha - J_{\parallel}(\rho_{\parallel}))t \quad (t \rightarrow \infty). \tag{8}$$

In view of the form (5), we call the region $\alpha > J_{\parallel}(\rho_{\parallel})$ with $\beta > \beta_c$ “maximal-current-divergent (MC-D) phase”, and $\alpha > J_{\parallel}(\rho_{\parallel})$ with $\beta < \beta_c$ “high-density-divergent (HD-D) phase”. On the other hand, the form (7) is not always valid in the divergent phase (see eq. (28) below). The main purpose of this paper is to determine the velocity V_{\parallel} for $\langle L_t \rangle \simeq V_{\parallel}t$ as well as the density profile in the divergent phase.

2.2 Backward sequential update

We now consider the discrete-time EQP with backward-sequential update (backward EQP): first a customer arrives with probability α , and the customer at the right end is extracted with probability β (if it exists). Then starting from the rightmost particle and

going sequentially to the left up to the leftmost particle, we move each particle forward with probability p if possible. For example

$$\begin{aligned} 101011 &\rightarrow 1011001 && \text{with probability } \alpha \times \beta \times p \times (1-p) \times p \times (1-p), \\ 111011 &\rightarrow 11111 && \text{with probability } (1-\alpha) \times (1-\beta) \times p \times p \times p, \\ \emptyset &\rightarrow \emptyset && \text{with probability } (1-\alpha) + \alpha \times \beta. \end{aligned} \quad (9)$$

In the first example of transitions (9), the customer on the second site can move to the rightmost site, thanks to the backward update. On the other hand, he/she cannot move in the parallel case, see the first example of Equation (3).

The current-density relation for the backward-sequential update¹ TASEP is [23]

$$J_-(\rho) = \frac{p\rho(1-\rho)}{1-p\rho}. \quad (10)$$

Simulation results imply that the critical line separating the parameter space of the EQP into convergent and divergent phases is given by

$$\alpha = J_-(\rho_-) = \begin{cases} \frac{\beta(p-\beta)}{p(1-\beta)} & (0 < \beta \leq \beta_c), \\ \frac{(1-\sqrt{1-p})^2}{p} & (\beta_c < \beta < 1), \end{cases} \quad \text{where } \rho_- = \begin{cases} \frac{p-\beta}{p(1-\beta)} & (0 < \beta \leq \beta_c), \\ \frac{1-\sqrt{1-p}}{p} & (\beta_c < \beta < 1), \end{cases} \quad (11)$$

with $\beta_c = 1 - \sqrt{1-p}$ as in the parallel case. The phase diagram is qualitatively similar to that of the parallel EQP (5), see Figure 2. In the special case $\beta = 1$ the system always has the stationary state $P(\emptyset) = 1$ and $P(\text{otherwise}) = 0$. Therefore we set $0 < \beta < 1$ in the following.

When $\alpha < J_-(\rho_-)$, we expect the system to converge to a stationary state, and the number of customers $\langle N_t \rangle$ decreases approximately linearly in time as

$$\langle N_t \rangle \sim (\alpha - J_-(\rho_-))t + \langle N_0 \rangle \quad (12)$$

while $t \lesssim \frac{\langle N_0 \rangle}{J_-(\rho_-) - \alpha}$ starting from a sufficiently large $\langle N_0 \rangle$ at time $t = 0$. The system length also exhibits a similar behavior

$$\langle L_t \rangle \sim \frac{\alpha - J_-(\rho_-)}{\rho_-}t + \langle L_0 \rangle. \quad (13)$$

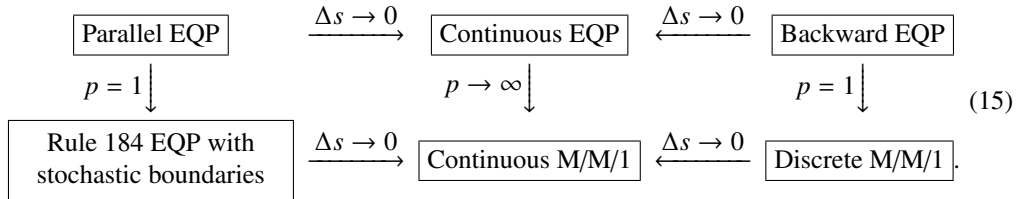
When $\alpha > J_-(\rho_-)$, we expect that the system does not have a stationary state and $\langle N_t \rangle$ and $\langle L_t \rangle$ diverge linearly in time. For $\langle N_t \rangle$, the form (12) is valid and we have the asymptotic behavior

$$\langle N_t \rangle \simeq (\alpha - J_-(\rho_-))t \quad (t \rightarrow \infty). \quad (14)$$

On the other hand, for the divergence of the length the form (13) is not always valid (see eq. (34) below).

2.3 Limits and special cases

The discrete-time EQPs have several known models as special cases or limits. The following diagram illustrates the relations between the various models:



¹Note that the sitewise and particlewise ordered updates [23] are identical here.

where Δs is the length of the discrete time step. (A more precise definition of the limit will be given below.)

2.3.1 Parallel update with $p = 1$

The deterministic hopping cases ($p = 1$) of the discrete-time EQPs correspond to two different processes. The bulk dynamics of the parallel EQP with $p = 1$ corresponds to the rule 184 cellular automaton with stochastic boundaries. It is still an EQP although the customer hopping is deterministic [6]. The MC-D and MC-C phases vanish in the phase diagram (Fig. 2). This case has an exact “dynamical state” in a matrix product form which enables us to derive asymptotic behaviors of the system length, the number of customers and the density profile in the limit $t \rightarrow \infty$ [18]:

- Divergent Phase ($\alpha > \beta/(1 + \beta)$):

$$\langle L_t \rangle = (\alpha - \beta + \alpha\beta)t + o(t), \quad \langle N_t \rangle = \frac{\alpha - \beta + \alpha\beta}{1 + \beta}t + o(t), \quad \rho_{x,t} \rightarrow \begin{cases} \frac{1}{1+\beta} & (x < 1), \\ 0 & (x > 1), \end{cases} \quad (16)$$

- Critical Line ($\alpha = \beta/(1 + \beta)$):

$$\begin{aligned} \langle L_t \rangle &= 2\sqrt{\frac{\beta t}{\pi(1 + \beta)}} + o(\sqrt{t}), \quad \langle N_t \rangle = 2\sqrt{\frac{\beta t}{\pi(1 + \beta)^3}} + o(\sqrt{t}), \\ \rho_{x\sqrt{t},t} &\rightarrow \frac{1}{1 + \beta} \text{erfc}\left(\frac{x}{2}\sqrt{\frac{1 + \beta}{\beta}}\right), \end{aligned} \quad (17)$$

- Convergent Phase ($\alpha < \beta/(1 + \beta)$):

$$\langle L_t \rangle \rightarrow \frac{\alpha}{\beta - \alpha - \alpha\beta}, \quad \langle N_t \rangle \rightarrow \frac{\alpha(1 - \alpha)}{\beta - \alpha - \alpha\beta}, \quad \rho_{jt} \rightarrow (1 - \alpha) \left(\frac{\alpha}{(1 - \alpha)\beta} \right)^j, \quad (18)$$

where erfc is the complementary error function $\text{erfc}(x) = \int_x^\infty e^{-y^2} dy$.

2.3.2 Backward-sequential update with $p = 1$

The backward EQP with $p = 1$ is equivalent to the discrete-time M/M/1 queueing process which is no longer an EQP as e.g. the state $\underbrace{1 \cdots 1}_N$ changes to $\underbrace{1 \cdots 1}_{N-1}$ when the customer at the server gets service. Thus no empty site appears between the leftmost customer and the server, i.e. we have always $N_t = L_t$, if the system starts from the empty chain. In the limit $t \rightarrow \infty$, the system shows different behavior, depending on the phase:

- Divergent Phase ($\alpha > \beta$):

$$\langle L_t \rangle = \langle N_t \rangle = (\alpha - \beta)t + o(t), \quad \rho_{x,t} \rightarrow \begin{cases} 1 & (x < 1), \\ 0 & (x > 1), \end{cases} \quad (19)$$

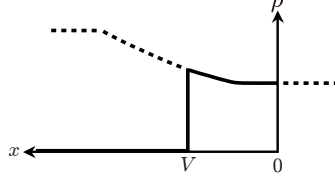


Figure 3: A schematic picture for the density profile in the divergent phase, where x is the rescaled position j/t . According to the injection probability (rate) α , the rarefaction wave is “cut” by the leftmost customer ($x = V$) and the server ($x = 0$).

- Critical Line ($\alpha = \beta$):

$$\langle L_t \rangle = \langle N_t \rangle = 2 \sqrt{\frac{\beta(1-\beta)}{\pi}} t + o(\sqrt{t}), \quad \rho_{x\sqrt{t},t} \rightarrow \text{erfc}\left(\frac{x}{2\sqrt{\beta(1-\beta)}}\right), \quad (20)$$

- Convergent Phase ($\alpha < \beta$):

$$\langle L_t \rangle = \langle N_t \rangle \rightarrow \frac{\alpha(1-\beta)}{\beta-\alpha}, \quad \rho_{jt} \rightarrow \left(\frac{\alpha(1-\beta)}{\beta(1-\alpha)}\right)^j. \quad (21)$$

2.3.3 Continuous-time update

Formally, in the continuous-time limit the probabilities α, β and p should be replaced by $\alpha\Delta s + o(\Delta s)$, $\beta\Delta s + o(\Delta s)$ and $\Delta s + o(\Delta s)$, respectively, and time t is rescaled as $t/\Delta s$. Then the continuous-time limits $\Delta s \rightarrow 0$ of both discrete-time EQPs yield the continuous-time EQP studied in [5]. The current-density relation for the continuous-time case is simply

$$J_{\text{cont}}(\rho) = p\rho(1-\rho), \quad (22)$$

and the phase diagram is given as

$$\alpha = J_{\text{cont}}(\rho_{\text{cont}}) = \begin{cases} \frac{\beta(p-\beta)}{p} & (0 < \beta \leq p/2), \\ \frac{p}{4} & (p/2 < \beta < 1), \end{cases} \quad \text{where } \rho_{\text{cont}} = \begin{cases} 1 - \frac{\beta}{p} & (0 < \beta \leq p/2), \\ \frac{1}{2} & (\beta > p/2). \end{cases} \quad (23)$$

The continuous-time M/M/1 queueing process is recovered by the continuous-time limits of the rule 184 case and the discrete-time M/M/1 queue. It is also obtained by the $p \rightarrow \infty$ limit of the continuous-time EQP.

3 Subphases in the divergent phase

We consider the TASEP on an infinite chain with the initial densities ρ_{right} (at sites $j < 0$) and ρ_{left} (at sites $j \geq 0$), where $\rho_{\text{left}} > \rho_{\text{right}}$. When the current J from left to right is given by a function of the density ρ , the rescaled density profile $\rho(x = j/t)$ is well-described by

$$\rho(x) \simeq \begin{cases} \rho_{\text{right}} & (x < f(\rho_{\text{right}})), \\ f^{-1}(x) & (f(\rho_{\text{left}}) > x > f(\rho_{\text{right}})), \\ \rho_{\text{left}} & (x > f(\rho_{\text{left}})) \end{cases} \quad (24)$$

with $f(\rho) = -\frac{dJ}{d\rho}$ [26]. We will see that, for the EQPs, the density profiles in the divergent phase are obtained by cutting this “rarefaction wave” as in Fig. 3.

3.1 Parallel case

From the current-density relation (4) for the parallel-update TASEP we have

$$f_{\parallel}(\rho) = -\frac{dJ_{\parallel}}{d\rho} = \frac{p(2\rho-1)}{\sqrt{1-4p\rho(1-\rho)}}, \quad f_{\parallel}^{-1}(x) = \frac{1}{2} + \frac{x}{2} \sqrt{\frac{1-p}{p(p-x^2)}}. \quad (25)$$

We assume that the (rescaled) density profile $\rho_{xt,t}$ (at site xt and time t) has the form

$$\rho_{xt,t} \simeq \begin{cases} 0 & (x > V, 0 > x), \\ \rho(x) & (V > x > 0), \end{cases} \quad (26)$$

where $\rho(x)$ is given by (24) with $\rho_{\text{right}} = \rho_{\parallel}$ and $\rho_{\text{left}} = 1$. This assumption is supported by simulation results. Here V is the velocity of the system length $\langle L_t \rangle \simeq Vt$.

Under the assumption (26) we have

$$t(\alpha - J^{\text{out}}) \simeq t \int_0^V \rho(x) dx, \quad (27)$$

where both sides are different expressions for the number of customers. Inserting $J^{\text{out}} = J_{\parallel}(\rho_{\parallel})$ (see Equation (5)) into Equation (27), we find the velocity

$$V = V_{\parallel} = \begin{cases} \frac{\alpha - J(\rho_{\parallel})}{\rho_{\parallel}} = \alpha \frac{p-\beta^2}{p-\beta} - \beta & \text{(I),} \\ 2p\alpha - p + 2\sqrt{p\alpha(1-p)(1-\alpha)} & \text{(II),} \\ \alpha & \text{(III),} \end{cases} \quad (28)$$

where

$$\begin{aligned} \text{I :} \quad & 0 < V_{\parallel} \leq f_{\parallel}(\rho_{\parallel}) & \text{i.e.} \quad & \frac{\beta(p-\beta)}{p-\beta^2} < \alpha \leq \frac{(p-\beta)^2}{p-2p\beta+\beta^2}, \\ \text{II :} \quad & f_{\parallel}(\rho_{\parallel}) < V_{\parallel} \leq f_{\parallel}(1) & \text{i.e.} \quad & \text{Max}\left(\frac{(p-\beta)^2}{p-2p\beta+\beta^2}, \frac{1-\sqrt{1-p}}{2}\right) < \alpha \leq p, \\ \text{III :} \quad & f_{\parallel}(1) \geq V_{\parallel} & \text{i.e.} \quad & p < \alpha \leq 1. \end{aligned} \quad (29)$$

Combing this and the form of ρ_{\parallel} given in Equation (5), we obtain five subphases in the divergent phase. In each phase the rescaled density $\rho_{xt,t}$ has a different form (Fig. 4):

$$\begin{aligned} \text{HD-D-I: } \rho_{xt,t} &\simeq \begin{cases} \rho_{\text{right}} & (V > x > 0), \\ 0 & (x > V), \end{cases} \\ \text{HD-D-II: } \rho_{xt,t} &\simeq \begin{cases} \rho_{\text{right}} & (v_1 > x > 0), \\ f_{\parallel}^{-1}(x) & (V > x > v_1), \\ 0 & (x > V), \end{cases} \quad \text{MC-D-II: } \rho_{xt,t} \simeq \begin{cases} f_{\parallel}^{-1}(x) & (V > x > 0), \\ 0 & (x > V), \end{cases} \\ \text{HD-D-III: } \rho_{xt,t} &\simeq \begin{cases} \rho_{\text{right}} & (v_1 > x > 0), \\ f_{\parallel}^{-1}(x) & (v_2 > x > v_1), \\ 1 & (V > x > v_2), \\ 0 & (x > V), \end{cases} \quad \text{MC-D-III: } \rho_{xt,t} \simeq \begin{cases} f_{\parallel}^{-1}(x) & (v_2 > x > 0), \\ 1 & (V > x > v_2), \\ 0 & (x > V), \end{cases} \end{aligned} \quad (30)$$

where

$$\rho_{\text{right}} = \rho_{\parallel}, \quad v_1 = f_{\parallel}(\rho_{\parallel}) = \frac{p(p-2\beta+\beta^2)}{p-2p\beta+\beta^2}, \quad v_2 = f_{\parallel}(1) = p, \quad f_{\parallel}^{-1}(x) = f_{\parallel}^{-1}(x). \quad (31)$$

The HD-D phase is divided into three phases: (I) plateau, (II) plateau-slope and (III) plateau-slope-plateau. On the other hand, the MC-D phase is divided into only two

phases: (II) slope and (III) slope-plateau. The plateau near the exit does not appear. Figures 5 and 6 show simulation results for the velocities and the density profiles, respectively, with parameters

$$(\alpha, \beta, p) = \begin{cases} (0.4, 0.3, 0.84) & \text{HD-D-I} & \circ \text{ (blue),} \\ (0.75, 0.3, 0.84) & \text{HD-D-I} & \triangle \text{ (red),} \\ (0.9, 0.3, 0.84) & \text{HD-D-III} & \times \text{ (purple),} \\ (0.55, 0.8, 0.84) & \text{MC-D-II} & \square \text{ (orange),} \\ (0.9, 0.8, 0.84) & \text{MC-D-III} & + \text{ (green).} \end{cases} \quad (32)$$

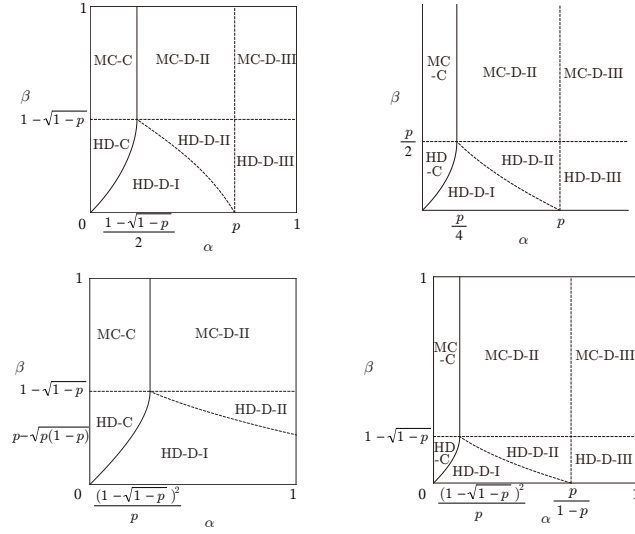


Figure 4: The subphases of the EQPs; the parallel EQP (top-left), the continuous-time EQP (top-right), the backward EQP with $\frac{1}{2} \leq p < 1$ (bottom-left) and the backward EQP with $0 < p < \frac{1}{2}$ (bottom-right).

3.2 Backward case

From the current-density relation (10) for the TASEP with the backward update we have

$$f_{\leftarrow}(x) := -\frac{dJ_{\leftarrow}}{d\rho} = -\frac{p(1-2\rho+p\rho^2)}{(1-p\rho)^2}, \quad f_{\leftarrow}^{-1}(x) = \frac{1}{p} - \frac{1}{p} \sqrt{\frac{1-p}{1+x}}. \quad (33)$$

As in the parallel-update case, we assume Equation (26) with $\rho(x)$ as in (24), $\rho_{\text{right}} = \rho_{\leftarrow}$ and $\rho_{\text{left}} = 1$. From Equation (27), we find that the velocity V_{\leftarrow} for the system length $\langle L_t \rangle \simeq V_{\leftarrow} t$ is given by

$$V_{\leftarrow} = \begin{cases} \frac{\alpha - J(\rho_{\leftarrow})}{\rho_{\leftarrow}} = \frac{p(1-\beta)}{p-\beta} \alpha - \beta & \text{(I),} \\ 2\sqrt{p(1-p)\alpha - p(1-\alpha)} & \text{(II),} \\ \alpha & \text{(III),} \end{cases} \quad (34)$$

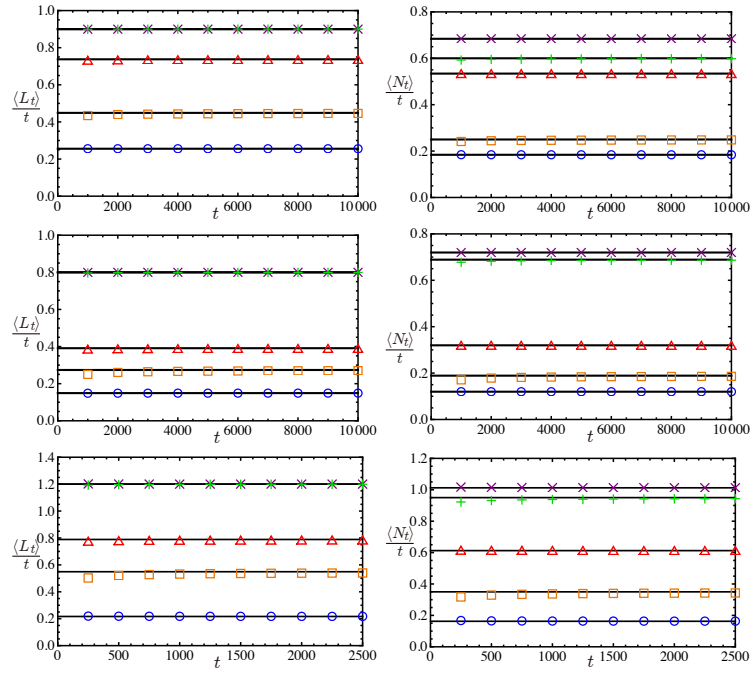


Figure 5: The growth velocities of the system size and the number of customers for the parallel (top), backward (middle) and continuous (bottom) EQPs. The simulation data were obtained by averaging 10^4 samples. We see that these agree with the lines corresponding to (28). The parameters are chosen as in Equations (32), (37) and (44).

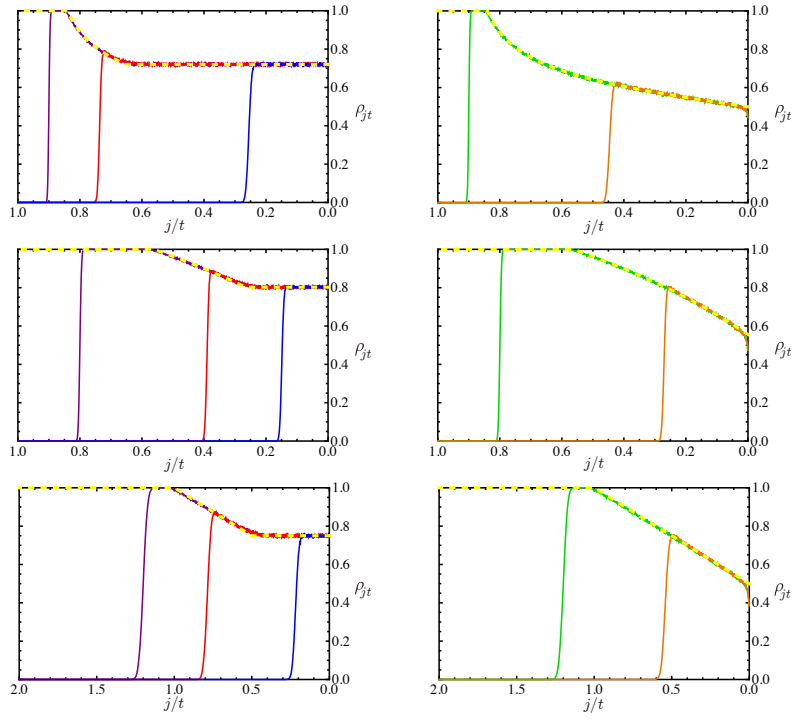


Figure 6: Rescaled density profiles ρ_{jt} of the parallel (top, $t = 10^4$), backward (middle, $t = 10^4$) and continuous-time (bottom, $t = 2500$) EQPs. The parameters are chosen as in Equations (32), (37) and (44). The simulation data were obtained by averaging 10^4 samples.

where

$$\begin{aligned}
\text{I : } & 0 < V_{\leftarrow} \leq f_{\leftarrow}(\rho_{\leftarrow}) & \text{i.e. } & \frac{\beta(p-\beta)}{p(1-\beta)} < \alpha \leq \frac{(p-\beta)^2}{p(1-p)}, \\
\text{II : } & f_{\leftarrow}(\rho_{\leftarrow}) < V_{\leftarrow} \leq f_{\leftarrow}(1) & \text{i.e. } & \text{Max}\left(\frac{(p-\beta)^2}{p(1-p)}, \frac{(1-\sqrt{1-p})^2}{p}\right) < \alpha \leq \frac{p}{1-p}, \\
\text{III : } & f_{\leftarrow}(1) > V_{\leftarrow} & \text{i.e. } & \frac{p}{1-p} < \alpha \leq 1.
\end{aligned} \tag{35}$$

When $\frac{1}{2} \leq p < 1$, the case D-III vanishes and the divergent phase is divided into three phases (Fig. 4). On the other hand, when $0 < p < \frac{1}{2}$, the structure of the subphases is qualitatively similar to the parallel case. The density profiles are given by Equation (30) with

$$\rho_{\text{right}} = \rho_{\leftarrow}, \quad v_1 = f_{\leftarrow}(\rho_{\leftarrow}) = \frac{p - 2\beta + \beta^2}{1 - p}, \quad v_2 = f_{\leftarrow}(1) = \frac{p}{1 - p}, \quad f^{-1}(x) = f_{\leftarrow}^{-1}(x). \tag{36}$$

Figures 5 and 6 show simulation results of the velocities and the density profiles, respectively, with parameters

$$(\alpha, \beta, p) = \begin{cases} (0.2, 0.1, 0.36) & \text{HD-D-I} & \circ (\text{blue}), \\ (0.4, 0.1, 0.36) & \text{HD-D-I} & \triangle (\text{red}), \\ (0.8, 0.1, 0.36) & \text{HD-D-III} & \times (\text{purple}), \\ (0.3, 0.6, 0.36) & \text{MC-D-II} & \square (\text{orange}), \\ (0.8, 0.6, 0.36) & \text{MC-D-III} & + (\text{green}). \end{cases} \tag{37}$$

3.3 Continuous-time case

From the current-density relation (22) for the continuous-time TASEP, we have

$$f_{\text{cont}}(\rho) := -\frac{dJ_{\text{cont}}}{d\rho} = p(2\rho - 1). \tag{38}$$

The velocity V_{cont} of the system length, the subphases and the density profiles can be obtained following the same procedure as for the parallel and backward EQPs, or simply by taking the continuous-time limits of the results for the two discrete cases:

$$V_{\text{cont}} = \begin{cases} \frac{\alpha - J(\rho_{\text{cont}})}{\rho_{\text{cont}}} = \frac{p}{p-\beta}\alpha - \beta & \text{(I),} \\ 2\sqrt{p\alpha} - p & \text{(II),} \\ \alpha & \text{(III),} \end{cases} \tag{39}$$

where

$$\text{I : } \quad 0 < V_{\text{cont}} \leq f_{\text{cont}}(\rho_{\text{cont}}) \quad \text{i.e. } \quad \frac{\beta(p-\beta)}{p} < \alpha \leq \frac{(p-\beta)^2}{p}, \tag{40}$$

$$\text{II : } \quad f_{\text{cont}}(\rho_{\text{cont}}) < V_{\text{cont}} \leq f_{\text{cont}}(1) \quad \text{i.e. } \quad \text{Max}\left(\frac{(p-\beta)^2}{p}, \frac{p}{4}\right) < \alpha \leq p, \tag{41}$$

$$\text{III : } \quad f_{\text{cont}}(1) > V_{\text{cont}} \quad \text{i.e. } \quad p < \alpha \leq 1. \tag{42}$$

The density profiles are given by Equation (30) with

$$\rho_{\text{right}} = \rho_{\text{cont}}, \quad v_1 = f_{\text{cont}}(\rho_{\text{cont}}) = p - 2\beta, \quad v_2 = f_{\text{cont}}(1) = p, \quad f^{-1}(x) = f_{\text{cont}}^{-1}(x) = \frac{1}{2} + \frac{x}{2p}. \tag{43}$$

Figures 5 and 6 show simulation results of the velocities and the density profiles, respectively, with parameters

$$(\alpha, \beta, p) = \begin{cases} (0.35, 0.25, 1) & \text{HD-D-I} & \circ \text{ (blue),} \\ (0.8, 0.25, 1) & \text{HD-D-I} & \triangle \text{ (red),} \\ (1.2, 0.25, 1) & \text{HD-D-III} & \times \text{ (purple),} \\ (0.6, 1, 1) & \text{MC-D-II} & \square \text{ (orange),} \\ (1.2, 1, 1) & \text{MC-D-III} & + \text{ (green).} \end{cases} \quad (44)$$

4 On the critical line

Since $\langle N_t \rangle$ and $\langle L_t \rangle$ converge to stationary values in the convergent phase, and diverge proportional to t in the divergent phase, we expect that they behave as

$$\langle X_t \rangle \sim t^{\gamma_X}, \quad 0 \leq \gamma_X \leq 1, \quad \text{for } X = L, N. \quad (45)$$

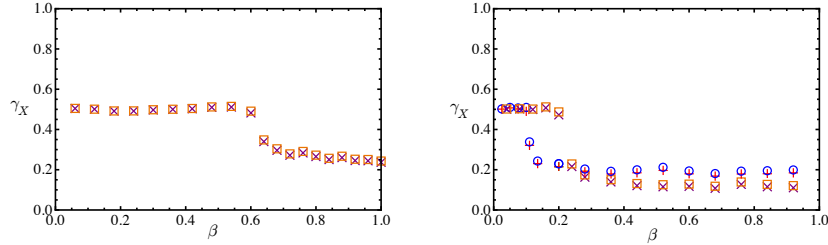


Figure 7: The exponents γ_X for the system length $X = L$ and the number of particles N on the critical lines of the parallel ($p = 0.84$, $\beta_c = 0.6$, left) and backward ($p = 0.36$, $\beta_c = 0.2$ and $p = 0.19$, $\beta_c = 0.1$, right) EQPs. The markers \square (orange) and \times (purple) correspond to γ_L and γ_N , respectively, for the parallel case with $p = 0.84$ and the backward case with $p = 0.36$, and \circ (blue) and $+$ (red) correspond to γ_L and γ_N , respectively, for the backward case with $p = 0.19$.

Under this assumption we have

$$\frac{\ln X_t - \ln X_{t/b}}{\ln b} \rightarrow \gamma_X \quad (t \rightarrow \infty), \quad (46)$$

for $X = L, N$. After verifying that the growth behavior is indeed well-described by power-laws of the form (45), we estimate the exponents γ_X by applying (46) to simulated samples with $b = 10$ and $t \leq 5 \times 10^5$. The number of samples for this estimation for each parameter set is basically 10^4 , but 10^6 or 5×10^6 samples were used for the backward EQP in the region $0.28 \leq \beta < 0.8$ and $\beta > 0.8$, respectively, because there fluctuations of L and N are very large. The results shown in Fig. 7 are consistent with the expectation $\gamma_L = \gamma_N$ everywhere on the critical line. This is supported by the observation that the total density $\rho_{\text{tot}} = \langle N_t \rangle / \langle L_t \rangle$ reaches quickly an almost stationary value which implies that $\gamma_L = \gamma_N$. More detailed results will be present in a future publication.

The critical lines of the EQPs consist of two parts: a curved and a straight line (Fig. 2). On the curved part, the simulation results indicate

$$\langle N_t \rangle, \langle L_t \rangle = O(\sqrt{t}). \quad (47)$$

The behavior of $\langle L_t \rangle$ and $\langle N_t \rangle$ on the straight part of the critical line is not so clear although diffusive behavior can be excluded. As Fig. 7 indicates, the exponents are smaller than on the curved part, i.e. $\gamma_L = \gamma_N < 1/2$. For the parallel case, $\gamma = 1/4$ (with large corrections near β_c) can not be excluded, but for the backward case, the exponents seems to depend on the value of p . For example, the exponents for $p = 0.19$ seem to be bigger than those for $p = 0.36$, see the right graph of Fig. 7. Our simulation results are not sufficient to determine conclusively the dependency of γ on the parameters, e.g. how it varies with β near β_c .

5 Conclusion

We have continued our studies of the exclusive queueing process (EQP) which extends the classical M/M/1 queueing process by incorporating the excluded volume effect. We have compared the behavior of the model with different update schemes (parallel, backward-sequential, continuous time). The phase diagrams are qualitatively similar, except for certain limiting cases.

The phase diagram of the EQP turns out to be rather rich. Here we have shown that the divergent phase is subdivided into up to 5 different subphases according to the parameter dependence of the current and the density profiles. The MC-D phase has two different subphases (the slope and plateau-slope phases), and the HD-D phase has three different subphases (the plateau, plateau-slope and plateau-slope-plateau phases).

In the divergent phase we have conjectured the analytic form of the density profiles which show good agreement with simulation results. The shapes of the rescaled profiles can be understood in terms of a rarefaction wave that is “cut” at both ends.

On the critical line separating the divergent from the convergent phase the length of the system grows sublinearly. Based on simulation results we find diffusive behavior on the curved part of the critical line (i.e. $\beta < \beta_c$) for all updates. In the special case $p = 1$ for the two discrete EQPs, the density profiles can be written in terms of the complementary error function as Equations (17) and (20). Identifying the density profile on the curved part for the EQPs with general values of p is one of problems that need to be clarified in the future.

The behavior on the straight part $\beta > \beta_c$ of the critical line is subdiffusive ($\gamma < 1/2$). However we could not clearly determine whether the exponent γ depends on the parameters, and more simulation data with sufficient accuracy are needed to determine the behavior on the straight part.

Acknowledgement

C Arita is a JSPS fellow for research abroad. The authors thank Kirone Mallick for useful discussions.

References

References

- [1] J. Medhi, *Stochastic Models in Queueing Theory*, Academic Press, San Diego (2003)

- [2] T.L. Saaty, *Elements of Queueing Theory With Applications*, Dover Publ. (1961)
- [3] W.J. Hopp, M.L. Spearman, *Factory Physics*, McGraw-Hill, Boston (2008)
- [4] A. Schadschneider, D. Chowdhury and K. Nishinari, *Stochastic Transport in Complex Systems: From Molecules to Vehicles*, Elsevier Science, Amsterdam (2010)
- [5] C. Arita, *Phys. Rev. E* **80**, 051119 (2009)
- [6] D. Yanagisawa, A. Tomoeda, R. Jiang and K. Nishinari, *JSIAM Lett.* **2**, 61 (2010)
- [7] K. Sugden, M.R. Evans, W.C.K. Poon, and N.D. Read, *Phys. Rev. E* **75**, 031909 (2007)
- [8] K. Sugden and M.R. Evans, *J. Stat. Mech.* (2007) P11013
- [9] M.R. Evans and K.E.P. Sugden, *Physica A* **384**, 53 (2007)
- [10] S. Dorosz, S. Mukherjee, and T. Platini, *Phys. Rev. E* **81**, 042101 (2010)
- [11] D. Johan, C. Erlenkämper, and K. Kruse, *Phys. Rev. Lett.* **108**, 258103 (2012)
- [12] A. Melbinger, L. Reese, and E. Frey, preprint arXiv:1204.5655 (2012)
- [13] M. Schmitt and H. Stark, *EPL* **96**, 28001 (2011)
- [14] C. Arita and D. Yanagisawa, *J. Stat. Phys.* **141**, 829 (2010)
- [15] B. Derrida, M. R. Evans, V. Hakim and V. Pasquier, *J. Phys. A* **26**, 1493 (1993)
- [16] M.R. Evans, N. Rajewsky and E.R. Speer, *J. Stat. Phys.* **95**, 45–96 (1999)
- [17] C. Arita and A. Schadschneider, *Phys. Rev. E* **83**, 051128 (2011)
- [18] C. Arita and A. Schadschneider, *Phys. Rev. E* **84**, 051127 (2011)
- [19] B. Derrida, *J. Stat. Mech.* P07023 (2007)
- [20] G.M. Schütz, *Exactly Solvable Models for Many-Body Systems Far from Equilibrium in Phase Transitions and Critical Phenomena vol 19.*, C. Domb and J. L. Lebowitz Ed., Academic Press, San Diego (2001)
- [21] R.A. Blythe and M.R. Evans, *J. Phys. A: Math. Gen.* **40**, R333 (2007)
- [22] T.M. Liggett, *Stochastic Interacting Systems: Contact, Voter and Exclusion Processes*, Springer, New York (1999)
- [23] N. Rajewsky, L. Santen, A. Schadschneider and M. Schreckenberg, *J. Stat. Phys.* **92** 151 (1998)
- [24] A. Schadschneider and M. Schreckenberg, *J. Phys. A: Math. Gen.* **26** L679 (1993)
- [25] M. Schreckenberg, A. Schadschneider, K. Nagel, and N. Ito, *Phys. Rev. E* **51**, 2939 (1995)
- [26] P.L. Krapivsky, S. Redner, and E. Ben-Naim, *A Kinetic View of Statistical Physics*, Cambridge University Press, Cambridge (2010)